

Negative angular dependent magnetoresistance in a zirconium/nickel bilayerL. H. Chou (周立信),^{1,2} S. C. Mai (麥軒誠) ^{1,3,4} W. Y. Li (李文淵),^{1,3,4} M. H. Lee (李明浩),^{1,5} C. Chuang (莊家翔),² and D. Qu (曲丹茹) ^{1,3,*}¹*Center for Condensed Matter Sciences, National Taiwan University, Taipei 10617, Taiwan*²*Department of Electronic Engineering, Chung Yuan Christian University, Taoyuan 320314, Taiwan*³*Center of Atomic Initiative for New Materials, National Taiwan University, Taipei 10617, Taiwan*⁴*Department of Physics, National Taiwan University, Taipei 10617, Taiwan*⁵*The Key Consortium of Electron Microscopy, National Taiwan University, Taipei 10617, Taiwan*

(Received 10 August 2023; revised 2 October 2023; accepted 31 October 2023; published 22 November 2023)

The electrical detection of spin and orbital angular momentum usually requires the utilization of a ferromagnetic metal (FM). When an angular momentum is generated in a light metal (LM), for example, through the orbital Hall effect, a bilayer system that consists of the LM/FM is commonly used to study the effect. In this work, by studying the magnetoresistance in the zirconium/nickel bilayer, a typical LM/FM bilayer structure, we observe a negative angular dependent magnetoresistance (ADMR) in the β scan direction. Through analysis, we exclude the contributions from the bulk effects and their combinations, such as the spin Hall effect and orbital Hall effect in zirconium, and the anomalous Hall effect in nickel. Instead, we attribute the negative ADMR to the interfacial spin-orbit coupling, which is caused by the imbalanced spin transmission and reflection at the interface. Our observation highlights the nontrivial contribution from the spin transport at the interface, which has often been overlooked in the study of the bulk effects in LM/FM bilayers.

DOI: [10.1103/PhysRevB.108.184422](https://doi.org/10.1103/PhysRevB.108.184422)**I. INTRODUCTION**

The pure spin current carries the maximal angular momentum with the minimal charge carriers. It efficiently transfers the angular momentum to a magnetic moment, perturbs, and eventually switches its magnetization. An electrical way of generating a pure spin current is through the spin Hall effect (SHE) [1]. In a material with strong spin-orbit coupling (SOC), a charge current generates a transverse spin current through the spin-orbit scattering. In recent years, beyond SHE, the orbital Hall effect (OHE) [2], in which a charge current generates a transverse orbital current that carries the orbital angular momentum, has been predicted and attracts intensive attention. Compared to the SHE, the OHE generally exists in all conducting metals regardless of its SOC strength. Moreover, the strength of the OHE is predicted to be orders of magnitude larger than the SHE for light metals (LMs), such as zirconium [3]. These aspects make the OHE a promising and more favorable electrical tool to generate the angular momentum.

Direct experimental techniques, such as the magneto-optical Kerr effect, which is sensitive to surface angular momentum accumulation, provides direct observations for the OHE in a single light $3d$ metal [4]. On the other hand, a wide range of studies on the OHE are based on indirect experimental techniques, such as harmonic [3], spin-orbit torque ferromagnetic resonance [5], hysteresis loop shift [6], and magnetoresistance (MR) [7] measurements. In the indirect techniques, a bilayer system consists of a light metal, and a

ferromagnetic metal (FM) is commonly used. But since the orbital current interacts with the magnetic moment through the spin-orbit interaction, the separation between the contribution from the orbital current and its spin counterpart remains an outstanding challenge.

Besides the competing bulk effects, for spin current generation and conversion in a bilayer or multilayer system, the interfacial spin transport also plays a vital role. Theoretical studies have predicted giant spin splitting at a heavy metal (HM)/FM interface [8] resembling the Rashba-Edelstein effect for an inversion symmetry-breaking system, which leads to a positive spin Hall magnetoresistance (SMR)-like behavior for the HM/FM bilayers [9]. On the other hand, as discussed in Refs. [10,11], an in-plane electric field is able to generate a spin current that flows perpendicularly to a HM/FM interface through the interfacial spin-orbit coupling (ISOC). This effect becomes prominent when the number of spin carriers that reflect from one side or transmit through the other side of the interface are different. The ISOC could induce a negative magnetic-field angular dependent magnetoresistance (ADMR) in the β scan direction compared to the positive SMR. A schematic illustration of the β scan ADMR is shown in Fig. 2(b), where the magnetoresistance is measured along the x -axis, under a magnetic field that rotates in the yz plane. Such ISOC-induced negative ADMR has been previously reported for the tantalum (Ta)/permalloy (Py) bilayer [12], where tantalum has a much larger resistivity compared with the permalloy.

A physical picture to describe the negative ADMR induced by the ISOC is shown in Figs. 1(a) and 1(b). When a charge current (x -axis) flows in a bilayer, a spin current that traverses across the interface (z -axis) is induced by the ISOC.

*danru@ntu.edu.tw

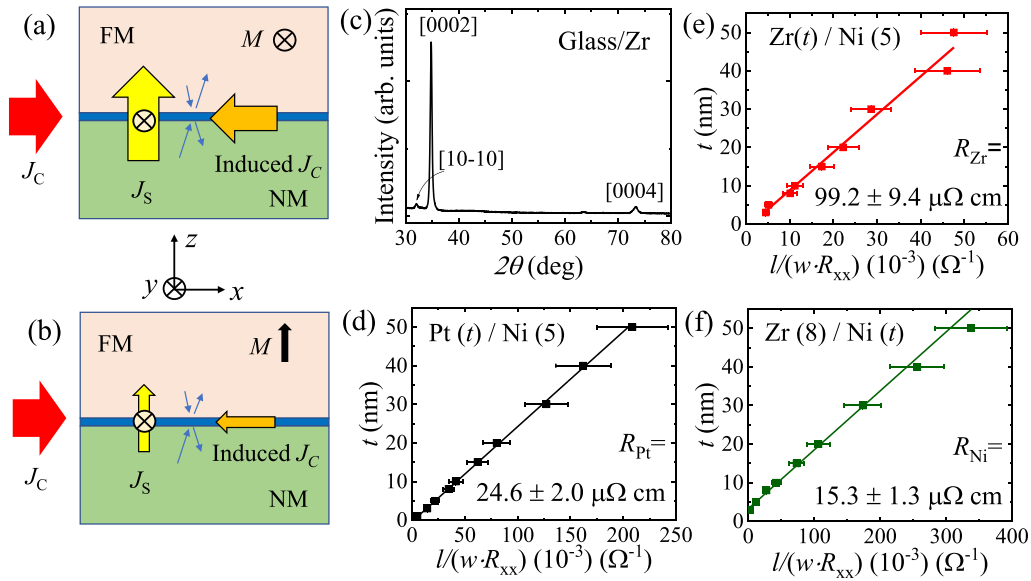


FIG. 1. Schematic illustration of the ISOC-induced negative ADMR. A spin current (J_S , yellow arrow) is generated and flows perpendicular to the interface upon a charge current (J_C , red arrow) injection. The J_S maximizes when the magnetization (M , black arrow) is (a) parallel and (b) perpendicular to the spin index on the y -axis. The reciprocal process of the ISOC then converts the interfacial spin current back to an induced charge current (Induced J_C , orange arrow) and results in a resistance change. (c) X-ray diffraction of the as-grown zirconium. Linear fittings of the thickness-dependent sheet resistance of (d) Pt(t)/Ni(5), (e) Zr(t)/Ni(5), and (f) Zr(8)/Ni(t).

It maximizes when the FM magnetization (M) is parallel to the spin index (M on the y -axis) and minimizes when they are perpendicular (M on the z -axis). The spin current is then converted back to an interfacial charge current through the inverse ISOC and flows in a direction opposite to the applied charge current. As a result, R_z (resistance R measured with M along the z -axis) is smaller than R_y (R measured with M along the y -axis) [12].

In this work, we study the MR for a bilayer system consisting of a light element (zirconium) and a ferromagnetic metal (nickel). In contrast to the positive SMR observed for Pt/Ni, we observe a negative ADMR for the Zr/Ni bilayer. The negative ADMR excludes the contribution from the bulk spin Hall or orbital Hall current from zirconium, the anomalous Hall effect from nickel, the interfacial Rashba-Edelstein effect at the Zr/Ni interface, and the cross contribution from these effects, since these effects result in a positive SMR-like magnetoresistance. By further excluding the contribution from the geometric size effect (GSE), we attribute the negative ADMR to the ISOC caused by the effective spin current generation and conversion across the Zr/Ni interface. Our results indicate that the ISOC could exist not only in a HM/FM bilayer, but also in a LM/FM bilayer. Therefore, when studying the spin current generation and conversion in a LM/FM system, not only the contributions from the bulk layers, but also the interfacial spin-orbit scatterings, which has been often overlooked, require careful examination.

II. RESULTS AND DISCUSSION

We fabricate a series of samples on glass substrates using magnetron sputtering. These samples include the room temperature-fabricated glass/Ni(t), glass/Pt(t)/Ni(5),

glass/Zr(t)/Ni(5), and glass/Zr(8)/Ni(t) films, where the numbers in parentheses indicate thickness in nanometers, with t representing a series of thicknesses between 1 nm and 50 nm. To prevent the top nickel from oxidation, we fabricate a 2-nm-thick Al_2O_3 capping layer for all samples. We first examine the crystallization of the zirconium films on glass substrate. As seen in Fig. 1(c), the as-grown zirconium already shows a textured hcp crystalline structure, with the [0002] and [0004] peaks observed within a 2θ range between 30° and 80° . The full width at half maximum (FWHM) of the [0002] peaks for the zirconium films is 0.39° . From the Scherrer equation $B(2\theta) = \lambda/(A \cos\theta)$, where $\lambda = 0.154$ nm is the x-ray wavelength, B is the FWHM, and 2θ is the angle between the x-ray source and the sample plane, we estimate the grain sizes for the zirconium films as 23.6 nm.

For all the thin-film samples studied in this work, we measure the resistance for each. For the bilayers of Zr(t)/Ni(5) and Pt(t)/Ni(5), we estimate the resistivity of zirconium and platinum, based on the parallel circuit model, $t = \frac{l}{wR_{xx}(t)}\rho_{\text{NM}} - \frac{l}{wR_{\text{FM}}}\rho_{\text{NM}}$. Here, t , $l = 4.75$ mm, and $w = 0.1$ mm are the thickness, length, and width, respectively, for the nonmagnetic (NM) zirconium layer. $R_{xx}(t)$ is the resistance of the bilayer. R_{FM} is the resistance of the FM nickel layer. ρ_{NM} is the resistivity of the NM layer. The slope of the linear fitting of t vs. $l/[wR_{xx}(t)]$ reveals ρ_{NM} . Similarly, we could obtain the resistivity of nickel from Zr(8)/Ni(t) samples. From the fittings, as shown in Figs. 1(d)–1(f), the resistivity of zirconium, platinum, and nickel are 99.6, 24.3, and 14.0 $\mu\Omega$ cm, respectively.

Next, we show the ADMR for these samples. Three geometries—the α , β , and γ scan geometries—as shown in Figs. 2(a)–2(c), are used to obtain the ADMR. For the ADMR measurement, a charge current $I = 0.1$ mA is applied, and a

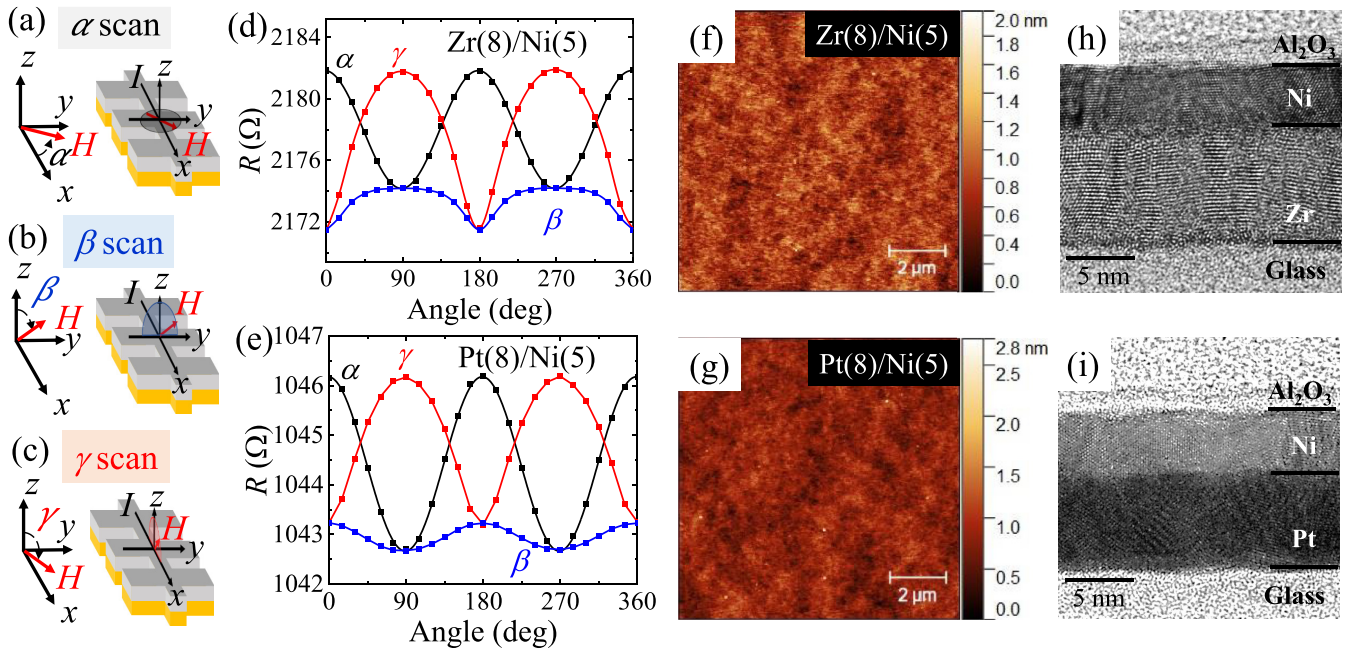


FIG. 2. Schematic illustration of the magnetoresistance measurement. In all cases, the charge current I is applied along the x -axis, the voltage V is measured in the same direction, while the magnetic field H is applied and scanned in the (a) xy plane (α scan), (b) zy plane (β scan), and (c) xz plane (γ scan). The angles α , β , and γ refer to the angles between H and the x -, z -, and z -axes, respectively. Angular-dependent magnetoresistance for (d) Zr(8)/Ni(5) and (e) Pt(8)/Ni(5), with the α scan, β scan, and γ scan marked in black, blue, and red, respectively. Surface morphology obtained through atomic force microscope for the $10\text{-}\mu\text{m} \times 10\text{-}\mu\text{m}$ area size (f) Zr(8)/Ni(5) and (g) Pt(8)/Ni(5). Cross-sectional transmission electron microscopy images for (h) Zr(8)/Ni(5) and (i) Pt(8)/Ni(5).

voltage is measured along the x -axis, while the magnetic field is applied and rotated in the xy plane (α scan), the zy plane (β scan), and the xz plane (γ scan). The α , β , and γ refer to the angle between the magnetic field and the x -, z -, and z -axes, respectively. The MR ratio for the α , β , and γ scans is defined as $\frac{R(\alpha, \beta, \text{ or } \gamma = 0^\circ) - R(\alpha, \beta, \text{ or } \gamma = 90^\circ)}{R(H=0)}$. Thus, an “M” (“W”) shape in the ADMR represents a negative (positive) ADMR ratio. The magnetization of the 50-nm-thick nickel thin film used in our study has a saturation magnetization (M_S) of 450 emu/cc. Throughout our measurements, to ensure the saturation of the nickel moment, we apply a magnetic field of 1.5 T to obtain the ADMR.

The ADMRs for Zr(8)/Ni(5) and Pt(8)/Ni(5) are shown in Figs. 2(d) and 2(e), respectively. In both cases, a 5-nm-thick nickel layer is utilized. The different resistance R for Zr/Ni and Pt/Ni is a result of the four times different resistivity of zirconium and platinum. For both Zr/Ni and Pt/Ni, the α scan ADMR is positive and the γ scan ADMR is negative, at about 3×10^{-3} . They are the result of the anisotropic magnetoresistance (AMR) in nickel originating from the s - d scattering [13]. For the β scan ADMR, Zr(8)/Ni(5) and Pt(8)/Ni(5) show opposite behaviors, which can be represented as shapes of “M” and “W”, respectively. For other thicknesses of zirconium and platinum, as shown in Figs. 3(a)–3(d), similar contrasting β scan ADMR results are observed. The shape of a “W”-like positive β scan ADMR ratio in Pt/FM has been previously extensively studied and is attributed to the SMR [14].

The negative β scan ADMR ratio observed in Zr/Ni is in sharp contrast to the positive ADMR ratio induced by

the spin Hall effect in Pt/Ni, the orbital Rashba-Edelstein effect (OREE) in CuO/Py [7], or the anomalous Hall effect in the iron-based ferromagnet [15]. Thus, the results exclude the contribution from the bulk spin current in zirconium, the orbital Rashba effect at the Zr/Ni interface, or the anomalous Hall effect (AHE) in nickel. A cross-contribution between these effects could also be excluded from a rough mathematic

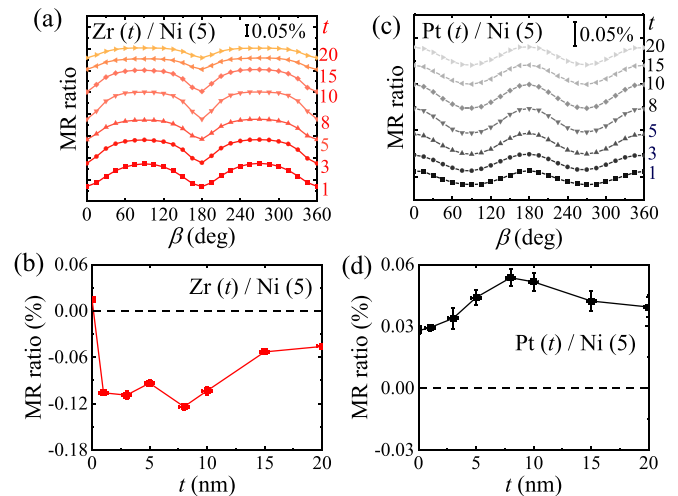


FIG. 3. NM layer thickness-dependent β scan angular dependent magnetoresistance. (a) Negative “M” shape ADMR for Zr(t)/Ni(5) and (c) positive “W” shape ADMR for Pt(t)/Ni(5). The summary of the thickness-dependent MR ratio for (b) Zr(t)/Ni(5) and (d) Pt(t)/Ni(5). Dashed lines indicate zero MR.

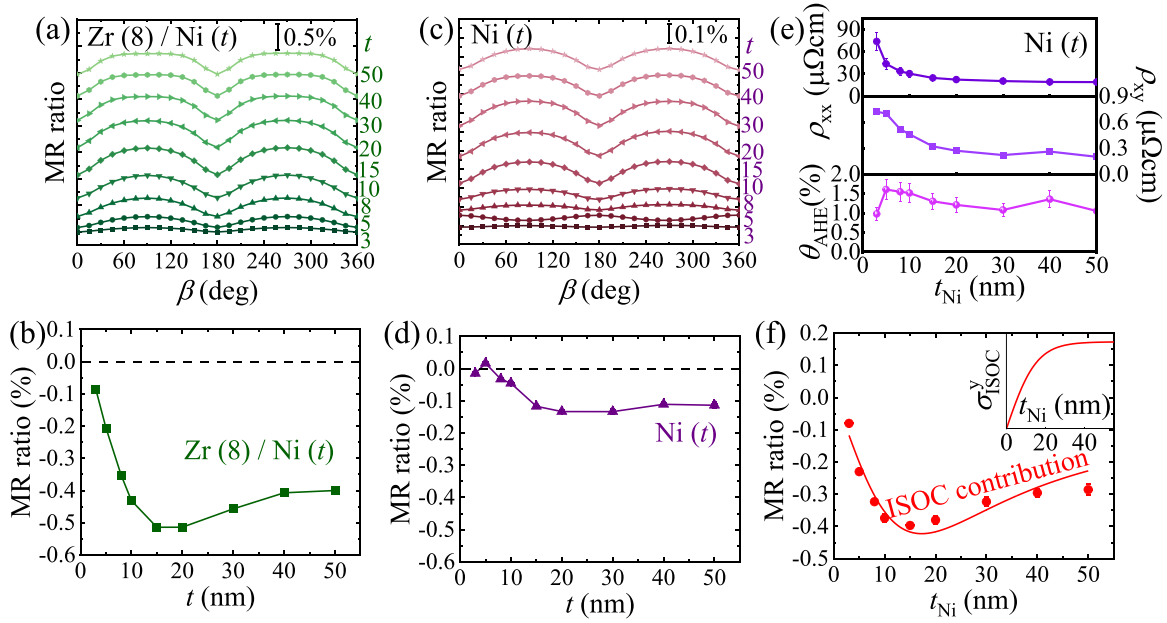


FIG. 4. FM layer thickness-dependent β scan angular dependent magnetoresistance. (a) Negative “M” shape ADMR for Zr(8)/Ni(t) and (c) “M” to “W” to “M” shape changing ADMR for Ni(t). The summary of the thickness-dependent MR ratio for (b) Zr(8)/Ni(t) and (d) Ni(t). The dashed lines indicate zero MR. (e) The longitudinal (upper panel) and transverse (middle panel) resistivity, and the anomalous Hall angle (lower panel) for Ni(t). (f) The ISOC contribution in Zr(8)/Ni(t) after removing the contribution from Ni(t). Inset: Nickel thickness-dependent interfacial spin filtering conductivity σ_{ISOC}^y inspired by Ref. [12].

estimation that $A^2 + B^2 + 2(A \cdot B) = (A + B)^2 \geq 0$. Here, A or B refers to the spin and charge conversion efficiency of the SHE, AHE, or OREE. A^2 and B^2 refer to the charge and spin conversions from the reciprocal effects. $2(A \cdot B)$ is the cross-contribution term. Thus, even if the cross term contributes a negative ADMR, when considering A^2 and B^2 together, the total contribution $A^2 + B^2 + 2(A \cdot B)$ to the MR is no smaller than zero. We also exclude the contribution from interfacial roughness to the reversed sign. We measure the $10\text{-}\mu\text{m} \times 10\text{-}\mu\text{m}$ area size surface morphology for Zr(8)/Ni(5) and Pt(8)/Ni(5) through atomic force microscopy. The results are shown in Figs. 2(f) and 2(g). The statistical analysis of the height reveals the same root mean square (RMS) roughness of 0.188 nm for each sample. Moreover, from the cross-sectional transmission electron microscopy (TEM) images for the two samples, as shown in Figs. 2(h) and 2(i), comparable interfacial quality is observed. Thus, the interfacial roughness could not be the reason of a reversed sign in the β scan ADMR.

Therefore, the only known effects left that contribute to a negative ADMR are the GSE in nickel originating from the additional MR anisotropy induced by a limited thickness for thin films [13] and the ISOC originating from the Zr/Ni interface caused by an imbalanced spin transmission and reflection from both sides of the interface [12]. Through symmetry analysis, cross-contributions from the SHE, OREE, and AHE with the ISOC are also canceled out by their Onsager conjugates [12].

To separate the contribution from the GSE and the ISOC, we measure the MR for two series of samples: Zr(8)/Ni(t) and Ni(t). Similar to the previous results of Zr(t)/Ni(5) and Pt(t)/Ni(5), the α scan and γ scan ADMRs reveal the AMR in nickel. As shown in Figs. 4(c) and 4(d), the β scan ADMR

ratio for nickel is negative and saturates for films thicker than 20 nm. This is the GSE in nickel. We notice for thin nickel film less than 10 nm, a positive contribution to the MR exists, which decays with increasing thicknesses. This is possibly caused by the anomalous Hall effect in nickel, which contributes a positive anomalous Hall MR (AHMR) [15]. The AHMR is maximum and overwhelms the GSE MR when the thickness of nickel is comparable to its spin diffusion length. As shown in Fig. 4(e), the anomalous Hall resistivity ρ_{xy} in nickel is enhanced by about four times for thinner films, while the AHE angle $\theta_{\text{AHE}} = \rho_{xy}/\rho_{xx}$ remains similar at about 1% to 1.5% for various thicknesses after considering the thickness-dependent resistivity ρ_{xx} .

For Zr(8)/Ni(t), as shown in Figs. 4(a) and 4(b), a five times larger negative ADMR is observed. Thus, the large negative MR ratio in Zr/Ni cannot be explained by the MR contribution from nickel alone. We attribute the additional source of the negative ADMR in the Zr/Ni bilayer to the ISOC. As mentioned earlier, the ISOC becomes prominent when the number of spin carriers that reflect from one side or transmit through the other side of the interface are different. In other words, when the resistivity of the two layers differs from each other, different numbers of electrons from different layers scatter at the interface and produce an effective net spin current that flows perpendicularly to the interface. The resistivity for the zirconium films used in this work is on the order of $100 \mu\Omega \text{ cm}$, while that for nickel is on the order of $14 \mu\Omega \text{ cm}$. Thus, a sizable net spin current is allowed to flow across the Zr/Ni interface through the ISOC.

By using the parallel circuit model, $\Delta R_{\text{MR}}^{\text{Zr/Ni}} = \frac{R_{\text{Zr/Ni}}}{R_{\text{Ni}}} \Delta R_{\text{MR}}^{\text{Ni}}$, where $\Delta R_{\text{MR}}^{\text{Ni}}$ is the MR ratio in nickel, $R_{\text{Zr/Ni}}$ is the resistance for the bilayer, and R_{Ni} is the resistance for nickel, we estimate

$\Delta R_{\text{MR}}^{\text{Zr/Ni}}$, the MR contributed from nickel to the bilayer. By subtracting $\Delta R_{\text{MR}}^{\text{Zr/Ni}}$ from the β scan ADMR in Zr(8)/Ni(t) samples, we obtain the negative ADMR contribution from the ISOC, as shown by the red dots in Fig. 4(f). We fit the ISOC MR $\frac{\Delta \rho_{xx}}{\rho_{xx}}$ vs. nickel thickness t_F using the ISOC model [12],

$$\frac{\Delta \rho_{xx}}{\rho_{xx}} = -\frac{\rho_F \rho_N^2 l_{\text{sf}}^N}{\rho_F t_N + \rho_N t_F} (\sigma_{\text{ISOC}}^y)^2 \left[\coth \left(\frac{t_N}{l_{\text{sf}}^N} \right) + \frac{\rho_F l_{\text{sf}}^F}{\rho_N l_{\text{sf}}^N} \coth \left(\frac{t_F}{l_{\text{sf}}^F} \right) - \frac{1}{\tilde{G} + \tanh \left(\frac{t_N}{l_{\text{sf}}^N} \right)} \right]. \quad (1)$$

Here, $\rho_N = 139 \mu\Omega \text{ cm}$ is the resistivity, $l_{\text{sf}}^N = 4.5 \text{ nm}$ [5] is the spin diffusion length, and $t_N = 8 \text{ nm}$ is the thickness for Zr. $\rho_F = 15 \mu\Omega \text{ cm}$ is the resistivity and $l_{\text{sf}}^F = 3.3 \text{ nm}$ [16] is the spin diffusion length for nickel. $\tilde{G} = 2G_{\uparrow\downarrow} l_{\text{sf}}^N \rho_N$ is a dimensionless mixing conductance and $G_{\uparrow\downarrow}$ is the spin mixing conductance at the Zr/Ni interface. σ_{ISOC}^y is the interfacial spin filtering conductivity [12]. By assuming a thickness-dependent σ_{ISOC}^y similar to Ref. [12], as shown in the inset of Fig. 4(f), which considers the thickness-dependent interfacial spin-orbit scattering strength, and by assuming an interface $G_{\uparrow\downarrow}$ of $10^{15} \Omega^{-1} \text{ m}^{-2}$, the fitted σ_{ISOC}^y is about $3.4 \times 10^5 \Omega^{-1} \text{ m}^{-1}$. This value falls in the wide range of the spin Hall conductivity reported for platinum [17]. This is a rough estimation of the ISOC strength at the Zr/Ni interface. When the referenced value l_{sf}^N , l_{sf}^F , or $G_{\uparrow\downarrow}$ is reduced (increased), σ_{ISOC}^y will be enhanced (reduced). Among the three referenced parameters, the change of l_{sf}^N affects σ_{ISOC}^y most.

From a symmetry point of view, the interfacial nickel, which has a weakened long-range exchange coupling, is different from the bulk nickel and could contribute to the ISOC. We also reverse the order of zirconium and nickel layers and fabricate glass/Al₂O₃(2)/Ni(50)/Zr(8)/Al₂O₃(2) multilayers to check the influence of interface roughness on the ISOC. For simplicity, we name the reversed sample Ni(50)/Zr(8). Compared to Zr(8)/Ni(50), the RMS roughness for Ni(50)/Zr(8) is reduced from 0.456 nm to 0.130 nm. It is accompanied by a reduction in the β scan ADMR ratio from -3.99×10^{-3} to -1.87×10^{-3} . For comparison, the RMS roughness and β scan ADMR ratio for the glass/Ni(50)/Al₂O₃(2) sample is 0.233 nm and

-1.14×10^{-3} , respectively. In either order of Zr(8)/Ni(50) or Ni(50)/Zr(8), the β scan ADMR ratio is larger than that of pure Ni(50), confirming the interfacial contribution. The results also suggest that a rougher interface could promote the ISOC strength. It is noticeable that the ISOC is previously used to describe the interfacial scattering for a heavy metal/FM bilayer. On the other hand, the negligible spin-orbit scattering in zirconium cannot contribute to the ISOC. Whether the orbital angular moment in zirconium plays a vital role at the interface scattering process remains an open question and awaits theoretical insights.

III. CONCLUSION

In summary, by utilizing the magnetoresistance measurement of the Zr/Ni bilayers, we observe a negative SMR-like behavior. We attribute the negative ADMR to the ISOC in the Zr/Ni bilayers. As mentioned earlier, there are reports [3,5] on the orbital torque generation in Zr/FM bilayers based on the opposite sign of the SHE and the OHE in zirconium. While the torque measurements are sensitive to the sign, the MR measurement, which is proportional to the square of the spin (orbital) Hall angle, shall reveal a positive SMR-like behavior regardless of the sign, if the SHE (OHE) plays a role. In our work, the negative ADMR observed in the Zr/Ni bilayer excludes the contribution from the bulk effects and their Onsager conjugates. In contrast, it highlights the important role of the interface spin-orbit scatterings in a bilayer or multilayer system. Thus, when separating various contributions in an LM/FM system, especially for two layers with different resistivity, the interfacial contribution cannot be neglected.

ACKNOWLEDGMENTS

We thank Ssu-Yen Huang and Xin Fan for fruitful discussions, Chao-Wei Chen for instrumentation support, and Ming-Wen Chu for TEM support. We acknowledge support by the Ministry of Science and Technology of Taiwan (Grant No. MOST 110-2112-M-002-047-MY3), the Center of Atomic Initiative for New Materials, National Taiwan University, and the Higher Education Sprout Project by the Ministry of Education in Taiwan.

[1] J. E. Hirsch, Spin Hall effect, *Phys. Rev. Lett.* **83**, 1834 (1999).
 [2] B. A. Bernevig, T. L. Hughes, and S.-C. Zhang, Orbitronics: The intrinsic orbital current in *p*-doped silicon, *Phys. Rev. Lett.* **95**, 066601 (2005).
 [3] Z. C. Zheng, Q. X. Guo, D. Jo, D. Go, L. H. Wang, H. C. Chen, W. Yin, X. M. Wang, G. H. Yu, W. He, H.-W. Lee, J. Teng, and T. Zhu, Magnetization switching driven by current-induced torque from weakly spin-orbit coupled Zr, *Phys. Rev. Res.* **2**, 013127 (2020).
 [4] Y.-G. Choi, D. Jo, K.-H. Ko, D. Go, K.-H. Kim, H. G. Park, C. Kim, B.-C. Min, G.-M. Choi, and H.-W. Lee, Observation of the orbital Hall effect in a light metal Ti, *Nature (London)* **619**, 52 (2023).

[5] R. Fukunaga, S. Haku, H. Hayashi, and K. Ando, Orbital torque originating from orbital Hall effect in Zr, *Phys. Rev. Res.* **5**, 023054 (2023).
 [6] T.-Y. Chen, Y.-C. Hsiao, W.-B. Liao, and C.-F. Pai, Tailoring neuromorphic switching by CuN_x-mediated orbital currents, *Phys. Rev. Appl.* **17**, 064005 (2022).
 [7] S. Ding, Z. Liang, D. Go, C. Yun, M. Xue, Z. Liu, S. Becker, W. Yang, H. Du, C. Wang, Y. Yang, G. Jakob, M. Kläui, Y. Mokrousov, and J. Yang, Observation of the orbital Rashba-Edelstein magnetoresistance, *Phys. Rev. Lett.* **128**, 067201 (2022).
 [8] S. Grytsyuk, A. Belabbes, P. M. Haney, H.-W. Lee, K.-J. Lee, M. D. Stiles, U. Schwingenschlögl, and A. Manchon,

- k-Asymmetric spin splitting at the interface between transition metal ferromagnets and heavy metals, *Phys. Rev. B* **93**, 174421 (2016).
- [9] Y. Du, S. Takahashi, and J. Nitta, Spin current related magnetoresistance in epitaxial Pt/Co bilayers in the presence of spin Hall effect and Rashba-Edelstein effect, *Phys. Rev. B* **103**, 094419 (2021).
- [10] V. P. Amin and M. D. Stiles, Spin transport at interfaces with spin-orbit coupling: Formalism, *Phys. Rev. B* **94**, 104419 (2016).
- [11] V. P. Amin and M. D. Stiles, Spin transport at interfaces with spin-orbit coupling: Phenomenology, *Phys. Rev. B* **94**, 104420 (2016).
- [12] M.-G. Kang, G. Go, K.-W. Kim, J.-G. Choi, B.-G. Park, and K.-J. Lee, Negative spin Hall magnetoresistance of normal metal/ferromagnet bilayers, *Nat. Comm.* **11**, 3619 (2020).
- [13] T. T. Chen and V. A. Marsocci, Transverse magnetoresistivity anisotropy measurements and the geometrical size effect in nickel thin films, *J. Appl. Phys.* **43**, 1554(1972).
- [14] H. Nakayama, M. Althammer, Y.-T. Chen, K. Uchida, Y. Kajiwara, D. Kikuchi, T. Ohtani, S. Geprägs, M. Opel, S. Takahashi, R. Gross, G. E. W. Bauer, S. T. B. Goennenwein, and E. Saitoh, Spin Hall magnetoresistance induced by a nonequilibrium proximity effect, *Phys. Rev. Lett.* **110**, 206601 (2013).
- [15] Y. Yang, Z. Luo, H. Wu, Y. Xu, R.-W. Li, S. J. Pennycook, S. Zhang, and Y. Wu, Anomalous Hall magnetoresistance in a ferromagnet, *Nat. Comm.* **9**, 2255 (2018).
- [16] K.-H. Ko and G.-M. Choi, Optical method of determining the spin diffusion length of ferromagnetic metals, *J. Magn. Magn. Mater.* **510**, 166945 (2020).
- [17] L. Zhu, L. Zhu, M. Sui, D. C. Ralph, and R. A. Buhrman, Variation of the giant intrinsic spin Hall conductivity of Pt with carrier lifetime, *Sci. Adv.* **5**, eaav8025 (2019).